Proceedings Paper:
Hua, Y, Neville, A orcid.org/0000-0002-6479-1871 and Barker, R orcid.org/0000-0002-5106-6929 (2018) Corrosion Behaviour of X65 Steels in Water-Containing Supercritical CO_2 Environments With NO_2/O_2. In: NACE 2018: Proceedings of the International Corrosion Conference and Expo Series. NACE CORROSION 2018 Conference and Expo, 15-19 Apr 2018, Phoenix, AZ, USA. National Association of Corrosion Engineers .

Corrosion behaviour of X65 steels in water-containing supercritical CO_2 environments with NO_2/O_2

Yong Hua
Institute of Functional Surfaces
School of Mechanical Engineering
University of Leeds, LS29JT
United Kingdom

Richard Barker
Institute of Functional Surfaces
School of Mechanical Engineering
University of Leeds, LS29JT
United Kingdom

Anne Neville
Institute of Functional Surfaces
School of Mechanical Engineering
University of Leeds, LS29JT
United Kingdom

ABSTRACT

Corrosion experiments were performed on X65 carbon steel in water-saturated supercritical CO_2 (SC-CO_2) and under-saturated SC-CO_2 conditions at 80 bar and 35℃ in the absence and presence of various combinations of NO_2 and O_2 ranging from 0-100 ppm and 0-1000 ppm, respectively. The purpose of the experiments was to understand the implications of the presence of these two species on both general and localized corrosion in likely conditions encountered during CO_2 transport.

The presence of 100 ppm NO_2 and 1000 ppm O_2 in water-saturated SC-CO_2 resulted in general corrosion rates reaching 0.3 mm/year after 48 hours and a localized corrosion rate of 6.8 mm/year, compared to 0.1 and 0.92 mm/year, respectively in the absence of both species. The final stages of testing considered corrosion rates in under-saturated SC-CO_2 with 100 ppm NO_2 and 1000 ppm O_2 at water contents between 0 and 1770 ppm. Although no corrosion occurred in dry conditions, increasing water concentration from 300 to 1770 ppm resulted in the general corrosion rates rising from 0.05 to 0.68 mm/year. However, there was no significant difference in the extent of localized corrosion observed with changing water content over this range, with values ranging between 0.5 and 0.6 mm/year.

Key words: corrosion, NO_2, O_2

INTRODUCTION

The corrosion in carbon steel pipelines transporting anthropogenic CO_2 from large sources has received considerable attention from many researchers.[1, 2, 3, 4, 5, 6] The possible presence of contaminants such as O_2, SO_x and NO_x in the CO_2 stream can influence and potentially accelerate the corrosion process.[1, 2, 3, 7, 8, 9, 10, 11, 12] Although carbon steels is a common and cost-effective pipeline material, it is highly susceptible to attack by corrosive impurities such as H_2O, CO_2, SO_2 and O_2.

With reference to literature within this subject area, most research efforts have been directed towards understanding the corrosion behaviour of X65 in dense phase CO_2 containing combinations of water, SO_2 or O_2 as impurities. Studies considering the effect of NO_2 individually or combined with O_2 on the corrosion behaviour of carbon steel in dense phase environments are rare and results have only been considered by a limited number of researchers.[2, 9, 13] The purpose of this work is to determine the susceptibility of UNS G15130 steels to water-containing supercritical CO_2 environments in the presence of NO_2 (50 or 100 ppm) and O_2 (1000 ppm) by measuring the general corrosion rates through the implementation of the weight loss method and surface profilometry to quantify the localized corrosion behaviour. Focus is directed towards three key areas; synergistic effects of NO_2 and O_2 in water-saturated conditions, the effects of solution replenishment on the corrosion rates determined in autoclave experiments, and the influence of water content in under-saturated conditions. A combination of Scanning Electron Microscopy (SEM), Raman spectroscopy and X-Ray Diffraction (XRD) is also implemented to understand the morphological and compositional changes in the corrosion products produced in the presence of NO_2 and O_2.

EXPERIMENTAL PROCEDURE

Test specimens were machined from carbon steel (UNS G15130) bar into discs with diameter of 25 mm and thickness of 6 mm. The chemical composition of the steel is provided in Table 1. Surface preparation consisted of wet-grinding the entire sample with up to 800 grit silicon carbide (SiC) abrasive paper, rinsing with distilled water, followed by acetone, high purity ethanol and drying gently with compressed air. Samples were then stored in a desiccator until required and weighed immediately before the experiment on an electronic balance with an accuracy of 0.001 mg before suspending inside the autoclave. Two samples were placed within the autoclave for each individual test.

Table 1: Elemental composition of UNS G15130 steel (wt. %)

C	**Si**	**Mn**	**P**	**S**	**Cr**	**Mo**	**Ni**
0.12	0.18	1.27	0.008	0.002	0.11	0.17	0.07
Cu	**Sn**	**Al**	**B**	**Nb**	**Ti**	**V**	**Fe**
0.12	0.008	0.022	0.0005	0.054	0.001	0.057	Balance

A schematic representation of the experimental system layout has been shown in a previous paper.[14] The entire system consists of a 1 liter capacity autoclave, temperature controller, a CO_2/NO_2/O_2 mixed cylinder, a liquid CO_2 cylinder and a series of valves for CO_2 flow control.

All tests were conducted in static conditions in either water-saturated supercritical CO_2, or with the water content below the calculated solubility limit (under-saturated) based on the work of Spycher et al.,[15] (i.e. the saturated water concentration in supercritical CO_2 at 35℃ and 8 MPa is 3437 ppm (in

mole)). In order to ensure the water-saturated CO_2 condition, 34000 ppm of water was introduced to the bottom of the autoclave (not in direct contact with the sample and approximately 10 times the saturation limit). Replenishment of the test fluid was achieved by releasing the solution from the autoclave and replacing the exact initial $CO_2/NO_2/O_2/H_2O$ mixture within the autoclave. This required de-pressurizing the system and re-pressurizing).

In terms of the autoclave operating procedure, distilled water was initially de-aerated by saturating the solution with CO_2 in a separate container for a minimum of 12 hours prior to testing. All the specimens were suspended within the autoclave on a non-conducting wire whilst also ensuring they were not in contact with the walls of the cylinder to prevent galvanic effects. The prepared, CO_2-saturated water was then delivered into the bottom of the autoclave at ambient pressure and temperature and sealed. All lines to the autoclave were then purged with CO_2 and evacuated to ensure the removal of initial traces of O_2 within the system. The required technical grade of $CO_2/O_2/NO_2$ mixture and liquid CO_2 was then transferred into the autoclave, heated and then pressurized to the correct temperature and pressure. The starting point of the test was taken from the time at which the autoclave reached the required temperature and pressure (35℃ and 8 MPa in this particular study).

At the end of each experiment, the specimens were dried thoroughly and photographed. The samples were subsequently chemically cleaned to remove all traces of corrosion products before weighing. The cleaning process consisted of wiping the surface with a cotton pad soaked in Clarke's solution (20 g antimony trioxide + 50 g stannous chloride + 1000 ml hydrochloric acid) in accordance with ASTM[1] Standard G1-03.[16] This was followed by rinsing the samples with distilled water and drying with compressed air. The mass loss due to corrosion was determined from the weight difference before exposure and after cleaning. The corrosion rates were calculated using Equation (1):

$$V_c = \frac{87600\Delta m}{\rho A t} \quad (1)$$

where V_c is the corrosion rate of the sample in mm/year, Δm is the mass loss in grams, ρ is the density of the sample in g/cm^3, A is the exposed area in cm^2 and t is the immersion time in hours.

Profilometry measurements were performed on samples after cleaning (scanning a 3 x 3 mm^2 area at a time) using a NP_{FLEX} 3D Surface Metrology System to quantify localized attack. The objective used was 2.5x with approximately a 3.5 mm working distance. The pit depth analysis was conducted in alignment with ASTM(1) Standard G46- 94.[17] The standard stipulates that an average of the 10 deepest pits should be used for pit damage characterization of the sample area. In some instances, samples were not cleaned with Clarke's solution and kept for analysis using either Scanning Electron Microscopy (SEM), Raman Spectroscopy or X-ray Diffraction (XRD).

As mentioned, three different stages of experimental tests were conducted. These comprised the following conditions:

- Stage 1: Examining the effect of individual impurities in the water-saturated environment (0-100 ppm NO_2 and 0-1000 ppm O_2 for 48 h)
- Stage 2: The process fluid replenishment (50 or 100 ppm NO_2 with 1000 ppm O_2 for 96 h with replenishment after 48 h)
- Stage 3: Under-saturated tests (water content from 0 – 1770 ppm in the presence of 100 ppm NO_2 and 1000 ppm O_2 for 48 h)

[1] ASTM International, 100 Barr Harbor Drive, West Conshohocken, PA 19428-2959.

The entire matrix of the experimental conditions for these three stages are provided in Table 2, 3 and 4. Table 2 (stage 1) studies the samples were exposed to water-saturated SC-CO_2 with various concentrations of NO_2 and O_2 (either separately or combined).

The matrix of the experiments for stage 2 is provided in Table 3. For these tests, the sample was exposed to water-saturated CO_2 environment in the presence of different concentrations of 50 or 100 ppm NO_2 and 1000 ppm O_2 as these were the most severe conditions encountered in the first stage of testing.

The final stage of testing considers the effect in the presence of 100 ppm NO_2 and 1000 ppm O_2 in an effort to determine the water content threshold required to avoid corrosion. For these series of tests, the last matrix of the experimental conditions is provided in Table 4. In these experiments the sample was exposed to under-saturated supercritical CO_2 conditions in the presence of 100 ppm NO_2 and 1000 ppm O_2 with water contents controlled at 1770, 1200, 650, 300 and 0 ppm. Baseline tests were also performed in the absence of NO_2 and O_2.

Table 2: Test matrix for studying the effect of individual impurity corrosion tests

Temperature (℃)	Pressure (MPa)	NO_2 ppm	O_2 ppm	H_2O (ppm (mole))	Materials	Immersion time (hours)
35	8	0	0	Water-saturated (34000 ppm water added into the autoclave)	X65	48
		50	0			
		100	0			
		0	1000			
		50	1000			
		100	1000			

Table 3: Test matrix for replenished solution corrosion tests

Temp. (℃)	Pressure (MPa)	H_2O (ppm (mole))	NO_2 (ppm (mole))	O_2 (ppm (mole))	Immersion time (hours)	
					Total	Replenishment time
35	80	Water-saturated (34000 ppm water added into the autoclave)	50	1000	96	Not replenished
						Replenished after 48 hours
			100			Not replenished
						Replenished after 48 hours

Table 4: Test matrix for under-saturated corrosion tests

Temperature (℃)	Pressure (MPa)	NO_2 ppm	O_2 ppm	H_2O ppm	Materials	Immersion time (hours)
35	80	0	0	1770	X65	48
		100	1000	1200		
				650		
				300		
				0		

RESULTS

Stage 1: The effect of individual and combined impurities on the corrosion behavior of carbon steel in water-saturated SC-CO_2 environments

Figure 1 provides the general corrosion rate and the profilometry measurements (in the form of a localized corrosion rate) extracted from the samples exposed to the water-saturated CO_2 environment at 35℃ and 8 MPa with various concentrations of NO_2 and O_2 present in the system for 48 h. The localized corrosion rates are based on the top 10 deepest surface pits, identified in alignment with ASTM[1] Standard G46-94.[17]

The general corrosion rate averaged 0.10 mm/year for samples exposed to the water-saturated environment in the absence of NO_2 and O_2, which can be considered as a baseline measurement. The addition of 50 and 100 ppm NO_2 only increased the corrosion rate to 0.17 and 0.23 mm/year, respectively. The introduction of 1000 ppm O_2 (no NO_2) reduced the general corrosion rate from the baseline test to 0.03 mm/year. The addition of both 50/100 ppm NO_2 and 1000 ppm O_2 increased the general corrosion rate in the system to around 0.29 and 0.30 mm/year, indicating that NO_2 can have an effect on the corrosion kinetics, even at low concentrations of 50 and 100 ppm. The results also indicate a notable synergistic effect between NO_2 and O_2 as the general corrosion rate in the presence of both species is greater than the sum of the corrosion rates when both are present individually.

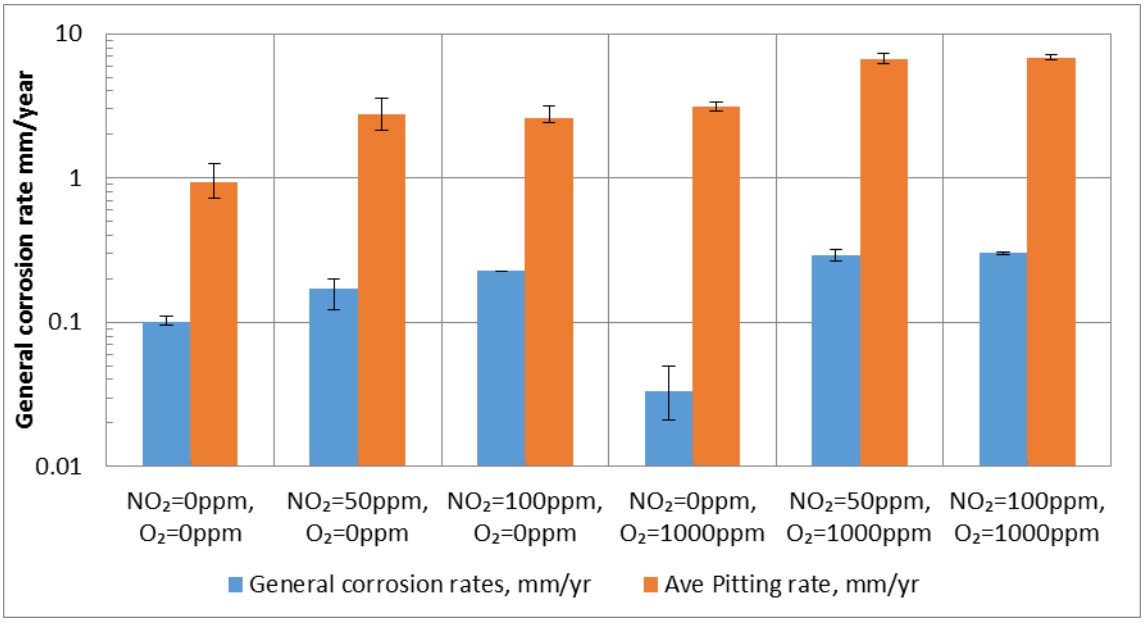

Figure 1: Average general corrosion and pitting rates of X65 carbon steel in water-saturated supercritical CO_2 environments containing varying concentrations of NO_2 and O_2 at 35℃ and 8 MPa for 48 hours

[1] ASTM International, 100 Barr Harbor Drive, West Conshohocken, PA 19428-2959.

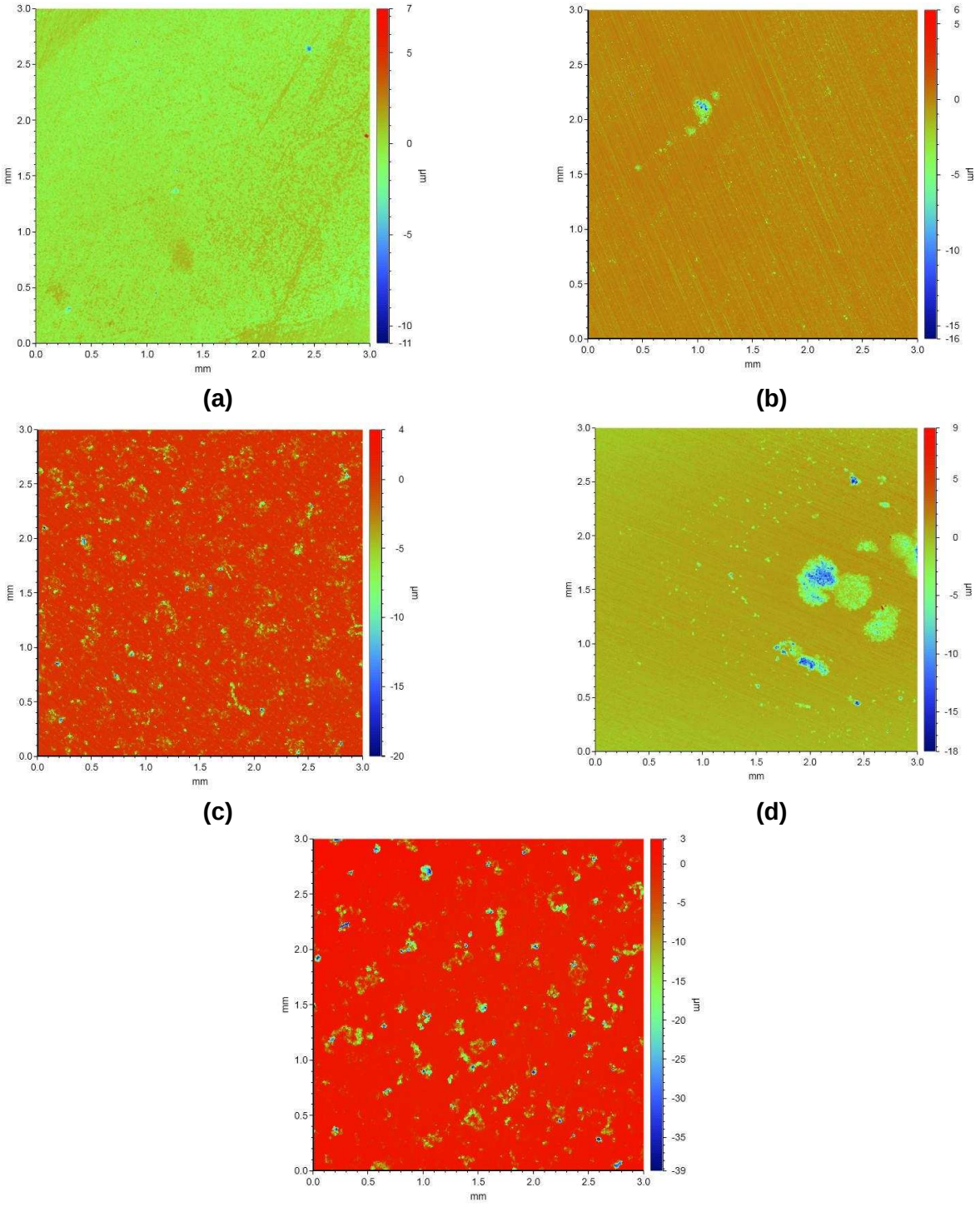

Figure 2: 2D profilometry images of X65 carbon steel exposed to water-saturated supercritical CO_2 environments containing varying concentrations of NO_2 and O_2 at 35℃ and 8 MPa for 48 hours (a) 0 ppm NO_2 and 0 ppm O_2, (b) 50 ppm NO_2 and 0 ppm O_2, (c) 100 ppm NO_2 and 0 ppm O_2, (d) 0 ppm NO_2 and 1000 ppm O_2 and (e) 100 ppm NO_2 and 1000 ppm O_2

In terms of the localized corrosion rates, the penetration from pitting or localized attack is over one order of magnitude greater than the general corrosion rates calculated through the implementation of

mass loss measurements. Examples of the profilometry images extracted are provided in Figure 2. The most severe localized attack was when NO_2 and O_2 were combined at a concentration of 100 ppm and 1000 ppm, respectively. This produced a penetration rate of 6.8 mm/year compared to 0.9 mm/year in the absence of both NO_2 and O_2.

Figure 3 provides the SEM images of the sample surfaces exposed to water-saturated supercritical CO_2 environments containing different levels of NO_2 and O_2 after 48 hours. In each instance the steel surface was found to be locally covered by various corrosion products. Figure 4 indicates the XRD patterns acquired through scans of over 1 cm^2 in area from each sample surface.

In the absence of NO_2 and O_2 in the system, the surface of the steel was locally covered by large, cubic crystals (Figure 3(a)) which were identified as $FeCO_3$ based on the XRD pattern shown in Figure 4. The addition of 1000 ppm O_2 inhibited the formation of crystalline $FeCO_3$ and formed an amorphous layer as shown in Figure 3(b). This layer mainly comprised of iron oxides and hydroxides which was identified in a previous study through the implementation of X-ray Photoelectron Spectroscopy (XPS).[14]

Addition of solely 50 or 100 ppm NO_2 changed the morphology of $FeCO_3$ and produced a corrosion product layer consisting of a large number of voids, as shown in Figure 3(c) for 100 ppm NO_2. Finally, the introduction of both 50 or 100 ppm NO_2 with 1000 ppm O_2 resulted in the formation of $FeCO_3$ covered by an amorphous top layer.

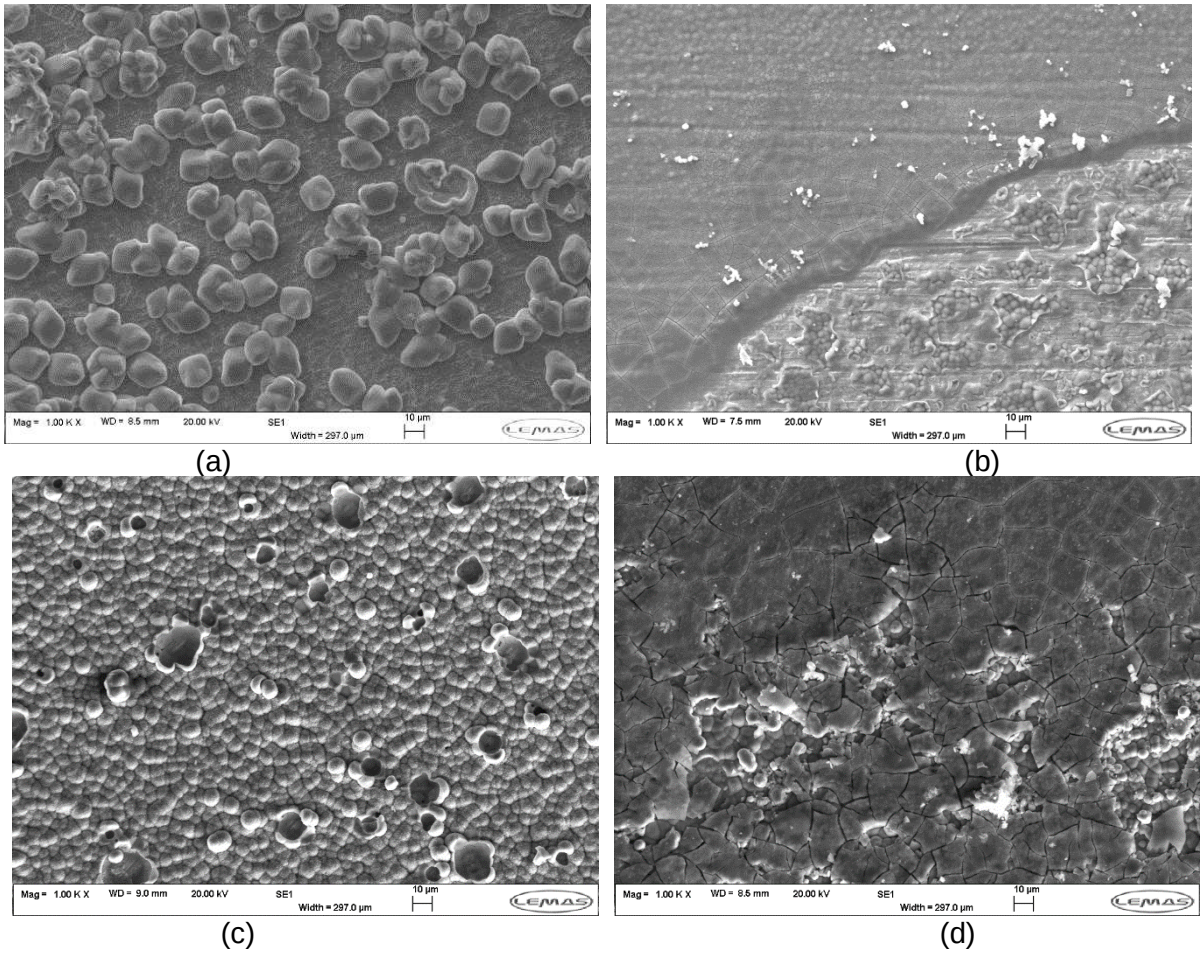

Figure 3: SEM images of surface morphology of corrosion products formed on X65 exposed to water-saturated CO_2 at 35℃ and 8 MPa after 48 hours for various impurities concentration (a) only water, (b) 1000 ppm O_2, (c) 100 ppm NO_2 and (d) 100 ppm NO_2 and 1000 ppm O_2.

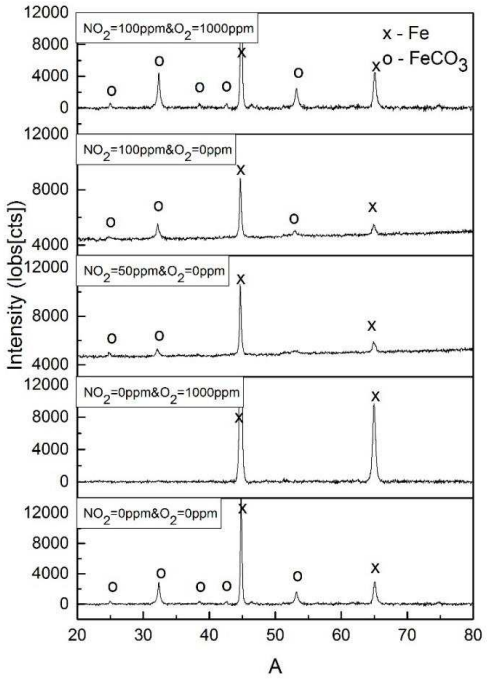

Figure 4: XRD patterns of X65 steel samples after exposure to water-saturated supercritical CO_2 phase at 35℃ and 8 MPa containing different concentrations of NO_2 and O_2

Stage 2: Effect of replenishing impurities in water-saturated CO_2 conditions

Another issue associated with experiments in closed vessels with low impurity concentrations is that significant levels of depletion (resulting in lower corrosion rates being observed) can occur in the system over the course of the experiment. To investigate the effect of impurity depletion, a series of tests were performed over 96 h in which the solution was or was not replenished.

The general and localized corrosion rates for the second stage of testing are provided in Figure 5 to indicate the effect of impurity replenishment. It is clear that replenishing the NO_2 and O_2 results in increased general corrosion rates. For the system containing 50 ppm NO_2 and 1000 ppm O_2, general corrosion rates increased from 0.17 to 0.26 mm/year by replenishing the solution, and the general corrosion rate in the system containing 100 ppm NO_2 and 1000 ppm O_2 increased by 40% from 0.19 to 0.32 mm/year. However, the localized corrosion rates showed no significant change as a result of renewing the solution. The localized corrosion rates provided in Figure 5 are approximately 3.1-3.3 mm/year in the presence of 50/100 ppm NO_2 and 1000 ppm O_2. This also indicates that, when compared with the localized corrosion rates after 48 h in Figure 1 under the same test conditions that the local penetration rate reduces markedly over the 96 h test duration. Example profilometry images are again provided in Figure 6 which show the high degree of localized attack.

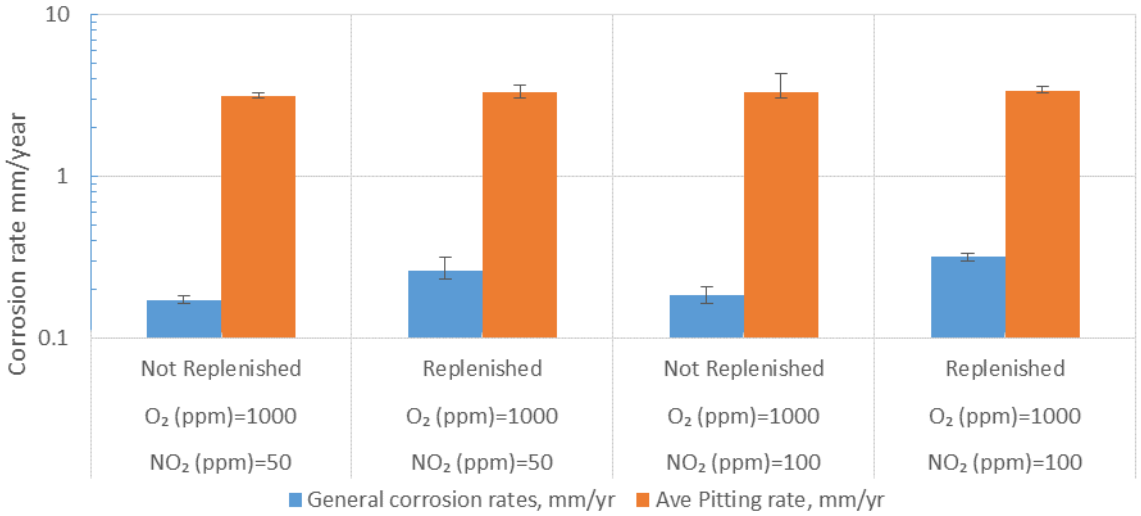

Figure 5: Average general corrosion and pitting rates of X65 carbon steel in the water-saturated CO_2 phase at 8 MPa and 35℃ for an exposure time of 96 hours, containing NO_2 (50 and 100 ppm) and 1000 ppm O_2, with and without impurity replenishment every 48 hours

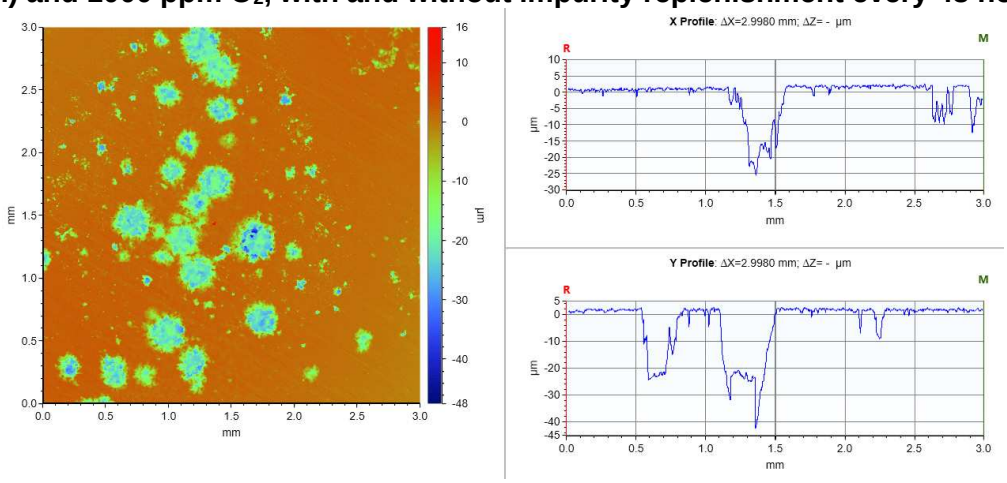

(a)

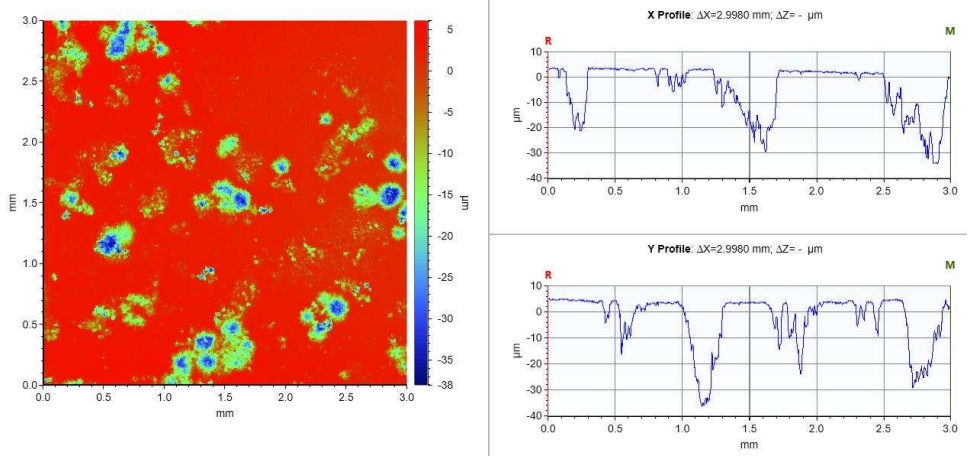

(b)

Figure 6: 2D profilometry images of X65 carbon steel exposed to water-saturated supercritical CO_2 environments at 35℃ and 8 MPa for 96 hours with or without replenishing solution after 48 hours containing (a) 100 ppm NO_2 and 1000 ppm O_2 – solution not replenished (b) 100 ppm NO_2 and 1000 ppm O_2 – solution replenished

The morphology and the level of visible corrosion product formed on the surface are similar with or without replenishing the impurities. Figure 7 shows an example of the SEM images for samples exposed to water-saturated supercritical CO_2 environments with replenishing 100 ppm NO_2 and 1000 ppm O_2 over 96 hours. It is interesting to note that the corrosion product are not uniformly distributed and the localized attack was clearly observed on the surface.

The XRD pattern of the samples exposed to the second stage of test environments is provided in Figure 8. A slight reduction in intensity for $FeCO_3$ was observed as a result of replenishing the impurities. The reduced intensity for $FeCO_3$ might indicate a lower quantity of $FeCO_3$ on the surface for the sample exposed to the replenished impurity and also suggest that the NO_2 and O_2 together can inhibit the formation of crystalline $FeCO_3$ on the surface, either due to increasing acidity of the condensed solution on the surface (as in the case of NO_2), or through oxidising ferrous ions into ferric ions (as in the case of O_2).[2]

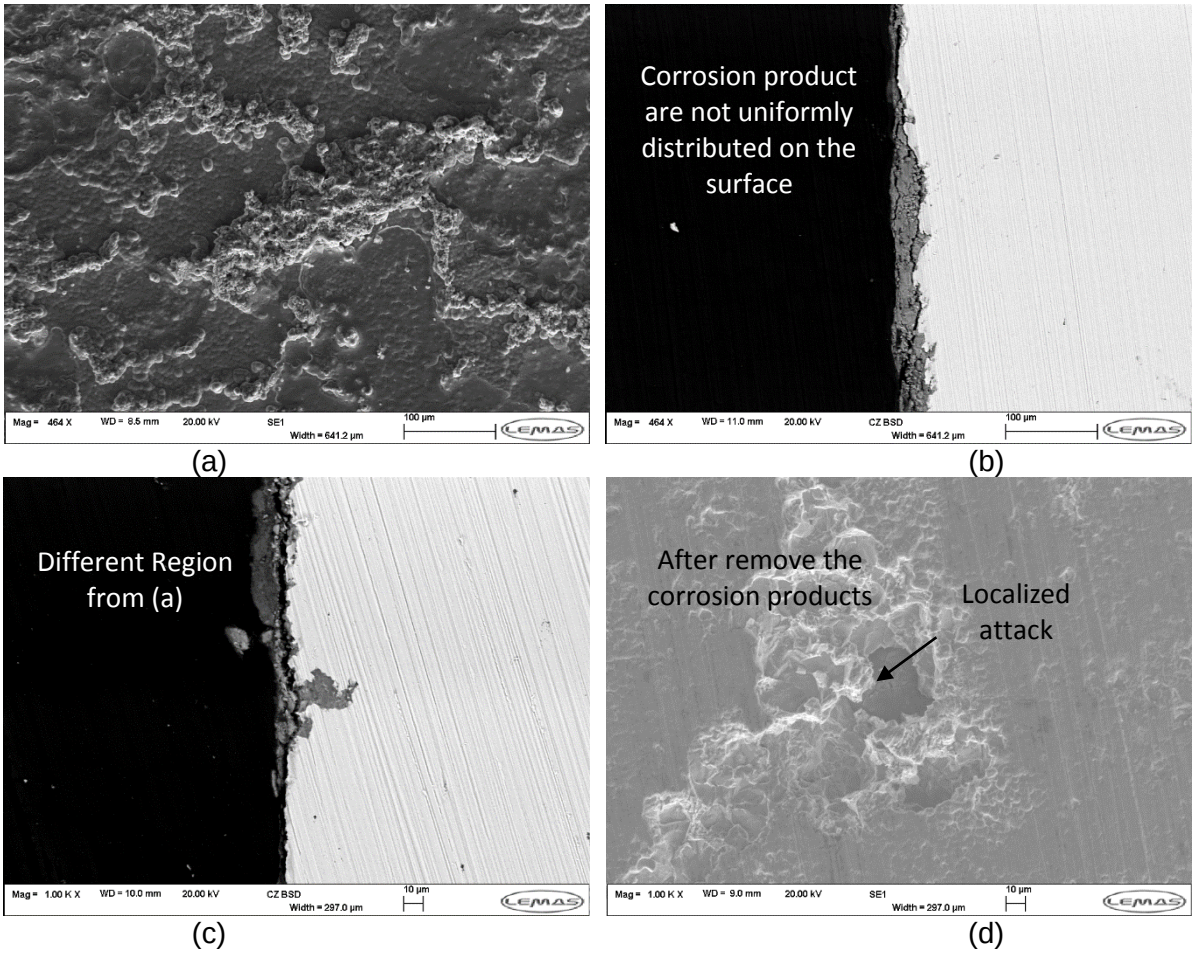

Figure 7: SEM images of surface morphology of corrosion products formed on X65 exposed to water-saturated CO_2 at 35℃ and 8 MPa for 96 hours with replenishing 100 ppm NO_2 and 1000 ppm O_2 after 48 hours.

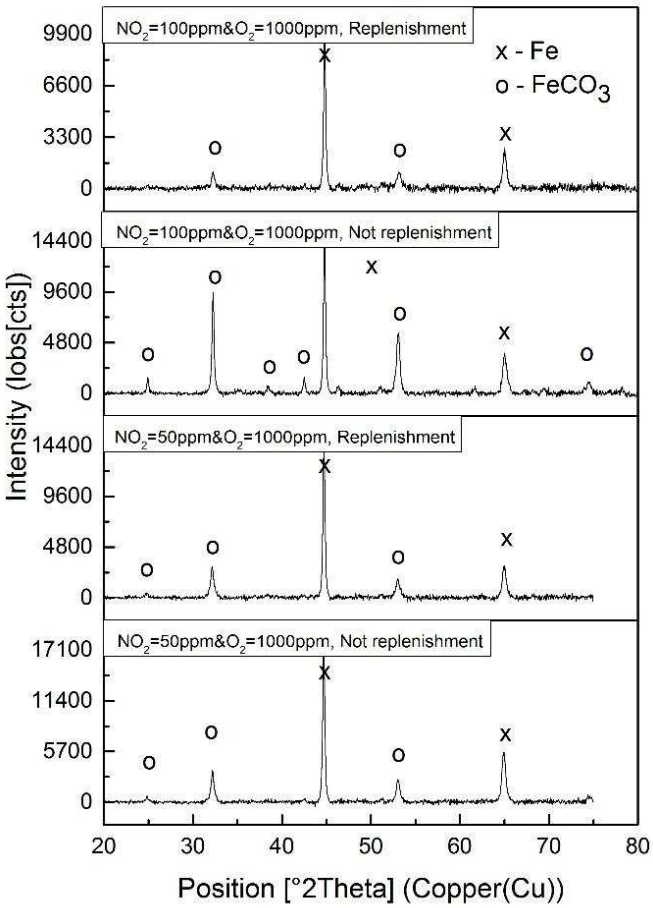

Figure 8: XRD patterns of samples exposed to water-saturated supercritical CO_2 phase at 35℃ and 8 MPa for 96 hours with and without replenishing 50/100 ppm of NO_2 and 1000 ppm of O_2 after 48 hours

Stage 3: Evaluation of general and localized corrosion in under-saturated CO_2 conditions for 100 ppm NO_2 and 1000 ppm O_2

When water is present in a SC-CO_2 system, either water-saturated conditions are created when the water content is above the solubility limit or the dense phase is under-saturated with water when the water content is below the solubility limit. One of the critical factors which influences the level of corrosion observed in an under-saturated system is the dissolved water content. Considering the conditions during the transport of CO_2 in pipelines, operators tend to dehydrate the CO_2 stream to specified levels below the solubility of water prior to transport. Therefore, it is also important to study the corrosion behaviour of X65 when exposed to under-saturated conditions in the supercritical CO_2 phase. This stage of testing considers this effect in the presence of 100 ppm NO_2 and 1000 ppm O_2 in an effort to determine the water content threshold required to avoid corrosion. For these series of tests, the last matrix of the experimental conditions is provided in Table 4. In these experiments the sample was exposed to under-saturated supercritical CO_2 conditions in the presence of 100 ppm NO_2 and 1000 ppm O_2 with water contents controlled at 1770, 1200, 650, 300 and 0 ppm. Baseline tests were also performed in the absence of NO_2 and O_2.

The measured general and localized corrosion rates of X65 when exposed to the under-saturated conditions at 35℃ and 8 MPa in the presence of 100 ppm NO_2/1000 ppm O_2 and 0 ppm NO_2/0 ppm O_2 are provided in Figure 9. For both environments, no measureable general and localized corrosion was recorded in dry conditions, while general and localized corrosion rates were 0.05 and 0.51 mm/year at a water content of 300 ppm for the 100 ppm NO_2/1000 ppm O_2 solution, respectively. In contrast to the tests without NO_2 and O_2, general corrosion rates were below 0-0.005 mm/year and no localized corrosion could be identified on the surface. This shows that a higher water content can be tolerated by the pure SC-CO_2 system compared to the system with NO_2 and O_2 impurities.

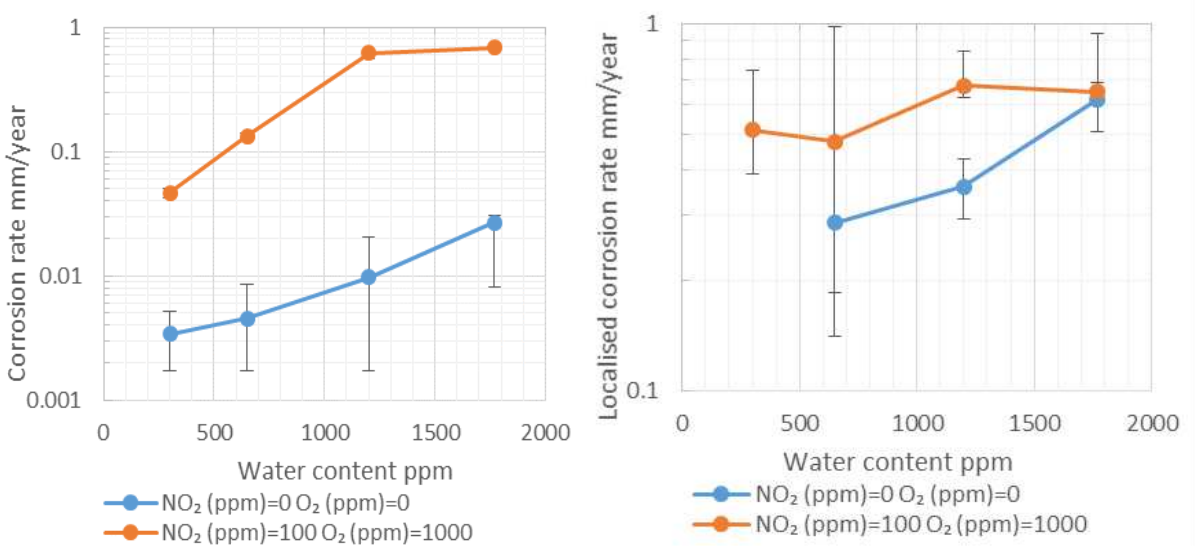

Figure 9: Average general corrosion rate and pitting corrosion rates of X65 carbon steel in under-saturated CO_2 phase at 8 MPa and temperature of 35℃ for an exposure time of 48 hours in the presence of 100 ppm NO_2 and 1000 ppm O_2. Data is presented on (a) general corrosion rate and (b) localized corrosion rate

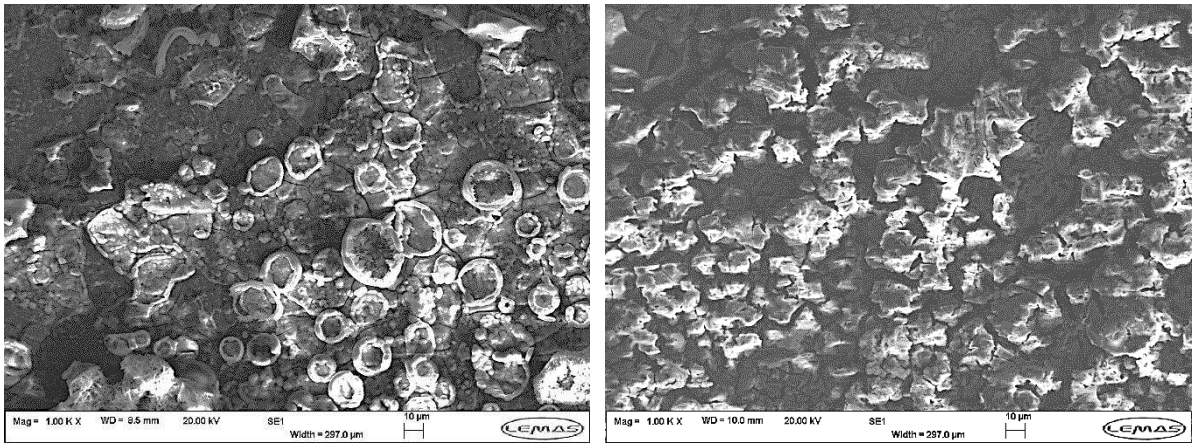

(a) **(b)**

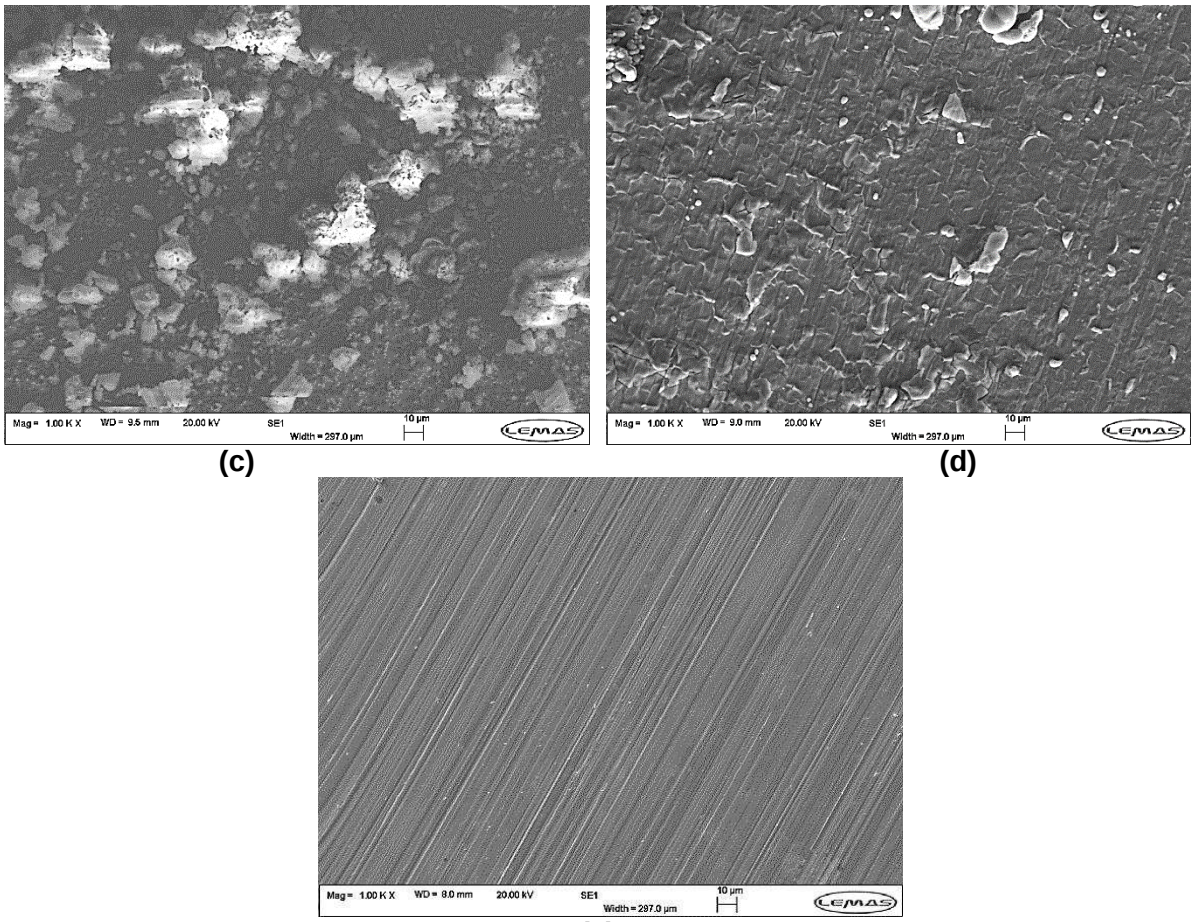

Figure 10: SEM images of surface morphology of corrosion products formed on X65 exposed to under-saturated CO_2 at 35℃ and 8 MPa after 48 hours in the presence of 100 ppm NO_2 and 1000 ppm O_2 (a) 1770 ppm, (b) 1200 ppm, (c) 650 ppm, (d) 300 ppm and (e) 0 ppm.

For the 100 ppm NO_2/1000 ppm O_2 system, the general corrosion rates increased from 0.05 mm/year to 0.68 mm/year as the water content rose from 300 ppm to 1770 ppm. However, the localized corrosion rate over this range did not change significantly averaging ~0.5 m/year, significantly lower than that recorded in the water-saturated system in Figure 1 by comparison.

SEM images of the sample surfaces provided in Figure 10 corroborate with the mass loss measurements in terms of the extent of corrosion product agreeing with the measured mass loss. For these experiments, the corrosion product was confirmed as $Fe(NO_3)_3$ according to the Raman measurements as shown in Figure 11. This suggests that the presence of NO_2 permits the formation of nitric acid within the condensed aqueous phase.

The influence of NO_2 and O_2 on corrosion product formation

Based on the collected XRD and Raman spectra from the steel surface in the collective presence and absence of NO_2 and O_2, it appears that two different corrosion products are predominately detected for water-saturated or under-saturated conditions.

For water-saturated environments, the XRD patterns showed only $FeCO_3$ crystals in the absence of 0 ppm NO_2 and 0 ppm O_2. The morphology of $FeCO_3$ crystals changed from cubic to globular through the addition of 50/100 ppm NO_2. Raman spectroscopy was used to provide the localized form of corrosion

product analysis. The results showed the corrosion products are mainly $FeCO_3$ in the presence of 50 or 100 ppm NO_2 with or without 1000 ppm O_2.

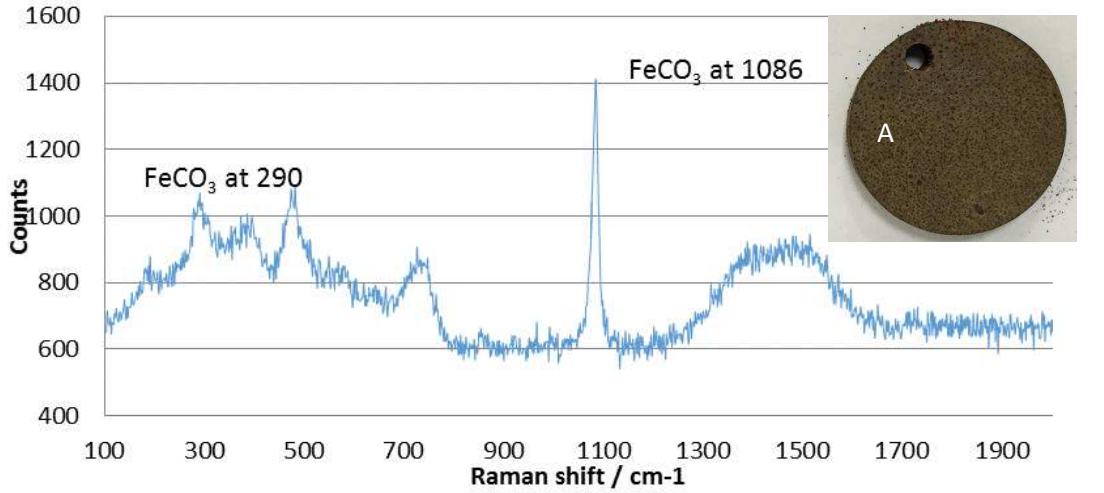

(a)

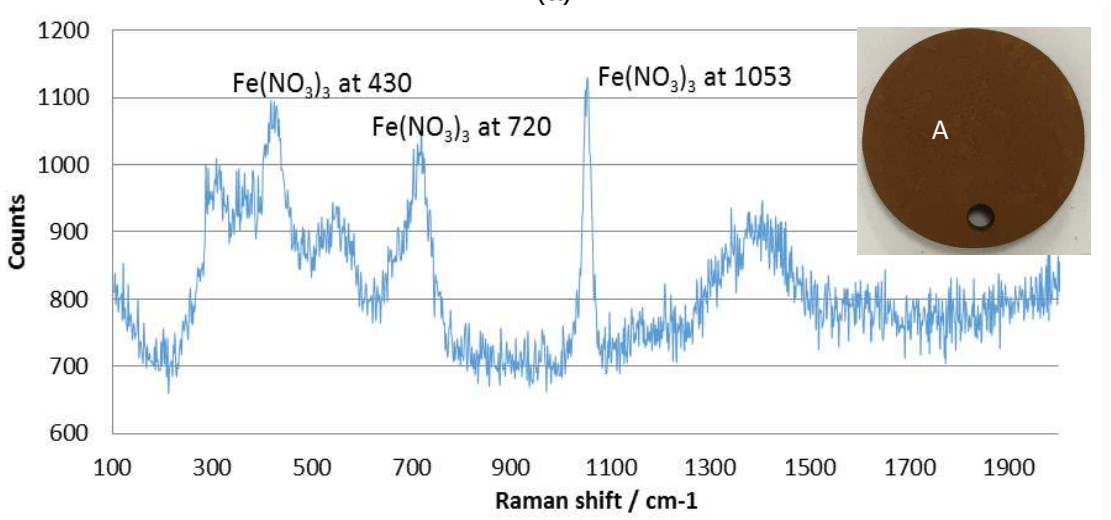

(b)

Figure 11: Raman spectra of samples exposed to (a) water-saturated and (b) under-saturated supercritical CO_2 phase at 35℃ and 8 MPa containing 100 ppm NO_2 and 1000 ppm O_2. Areas scanned on the steel surface are representative of those depicted in (A).

For under-saturated environments, in the system containing 100 ppm NO_2 and 1000 ppm O_2, no $FeCO_3$ crystals were detected by XRD or Raman. Instead the presence of $Fe(NO_3)_3$ was detected (peaks at 430 cm^{-1}, 720 cm^{-1} and 1053 cm^{-1} in Figure 11) and fully covered the entire steel surface. The possible reactions can be described by the following reactions:

The presence of CO_2 and NO_2 is believed to dissolve into the water rich phase to form carbonic acid and nitric acid which dissociated via the following reactions:

$$H_2O + 3NO_2 \rightarrow NO + 2HNO_3 \quad (2)$$

$$HNO_3 \rightarrow H^+ + NO_3^- \quad (3)$$

$$CO_2 + H_2O \rightarrow H_2CO_3 \quad (4)$$

$$H_2CO_3 + 2e^- \rightarrow H_2 + 2HCO_3^- \quad (5)$$

$$2HCO_3^- + 2e^- \rightarrow H_2 + 2CO_3^{2-} \quad (6)$$

The possible cathodic reactions included the reduction of hydrogen ions (produced from both carbonic and nitric acid) and the reduction reaction of O_2 can accelerate the cathodic reactions:

$$2H^+ + 2e^- \rightarrow H_2 \quad (7)$$

$$O_2 + 4H^+ + 4e^- \rightarrow 2H_2O \quad (8)$$

$FeCO_3$ and $Fe(NO_3)_3$ can then form via their respective precipitation processes:

$$Fe^{2+} + CO_3^{2-} \rightarrow FeCO_3 \quad (9)$$

$$Fe^{3+} + 3NO_3^- \rightarrow Fe(NO_3)_3 \quad (10)$$

Sun et al.,[9] suggested that $Fe(NO_3)_3$ may exist as an unstable corrosion product and can facilitate the formation of iron oxide (Fe_2O_3) via the following reaction. However, this cannot be confirmed in this study:

$$4Fe(NO_3)_3 \rightarrow 2Fe_2O_3 + 12NO_2 + 3O_2 \quad (11)$$

However, the results here corroborate with Sun et al.,[9, 10] given the detection of $FeCO_3$ and $Fe(NO_3)_3$ despite their experiments being performed at much higher O_2 and NO_2 contents. In their tests, $Fe(NO_3)_3$ and Fe_2O_3 were reported to have formed on X65 in the presence of 1000 ppm NO_2 and 1000 ppm O_2 after 72 hours exposure time. However, Fe_2O_3 was not observed in this study possibly due to the lower NO_2 content (100 ppm). The results here also suggest that a noticeable synergy exists between the two species resulting in the slight enhancement of the rate of material dissolution, particularly at under-saturated conditions.

CONCLUSIONS

The research presented has focused towards quantifying the extent of the general corrosion and localized corrosion of X65 carbon steel in 3 different environments: water-saturated, replenished solution and under-saturated supercritical CO_2 environments containing various levels of nitrogen oxide (NO_2) and oxygen (O_2), representative of dense phase anthropogenic carbon dioxide (CO_2) transport. Tests were conducted at a pressure of 8 MPa and a temperature of 35℃ for 48 hours in an effort to understand carbon steel performance/susceptibility, but also to identify the potential synergistic effect between NO_2 and O_2. From this study the following conclusions can be made:

- In water-saturated conditions containing various levels of NO_2 and O_2, general corrosion rates of carbon steel was 0.1 mm/year in the absence of NO_2 and O_2. The general corrosion rate of carbon steel increased from 0.1 to 0.3 mm/year by addition of 100 ppm NO_2 and 1000 ppm O_2.
- In water-saturated conditions containing 50 or 100 ppm NO_2 and 1000 ppm O_2, the highest localized corrosion rates with ranged between 6.6 and 6.8 mm/year. The localized corrosion

rates were over one order of magnitude higher than the general corrosion rates in all the environments, with a noticeable synergistic effect being observed between NO_2 and O_2 in terms of enhancing the localized dissolution of carbon steel.

- General corrosion rates increased with the replenishment of the process fluids, although the localized corrosion rates showed no significant change as a result of replacing the test solution.
- In under-saturated conditions containing 100 ppm NO_2 and 1000 ppm O_2, the general corrosion rates increased from 0 to 0.68 mm/year as the water content was increased from 0 to 1770 ppm. However, the localized corrosion rate was not influenced significantly by water content variation providing the water content was below the solubility limit.
- The formation of iron nitrate ($Fe(NO_3)_3$) as well as iron carbonate ($FeCO_3$) was detected on the steel surface in systems containing NO_2 and O_2, suggesting that NO_2 permits the formation of nitric acid within the condensed aqueous phase on the steel surface.

ACKNOWLEDGEMENTS

Special thanks go to Johnston Shaun from Wood Group Kenny and Alex Hunt from WOODVIEW Technology for their invaluable advice. This research was financially supported by innovate UK.

REFERENCES

1. Y.-S. Choi, S. Nešić, and D. Young, Effect of impurities on the corrosion behavior of CO_2 transmission pipeline steel in supercritical CO_2−water environments. Environmental Science & Technology, 2010. 44(23): p. 9233-9238.
2. A. Dugstad, M. Halseid, and B. Morland, Effect of SO_2 and NO_2 on corrosion and solid formation in dense phase CO_2 pipelines. Energy Procedia, 2013. 37: p. 2877-2887.
3. Y. Xiang, Z. Wang, X.X. Yang, Z. Li, and W.D. Ni, The upper limit of moisture content for supercritical CO_2 pipeline transport. The Journal of Supercritical Fluids, 2012. 67: p. 14-21.
4. Y. Hua, R. Barker, and A. Neville, Effect of temperautre on the critical water content for general and localised corrosion of X65 carbon steel in the transport of supercritical CO_2. The International Journal of Greenhouse Gas Control, 2014. 31: p. 48-60.
5. Y. Hua, R. Barker, and A. Neville, Comparison of corrosion behaviour for X-65 carbon steel in supercritical CO_2-saturated water and water-saturated/unsaturated supercritical CO_2 The Journal of Supercritical Fluids, 2015. 97: p. 224-237.
6. Barker, R., Y. Hua, and A. Neville, Internal corrosion of carbon steel pipelines for dense-phase CO2 transport in carbon capture and storage (CCS)–a review. International Materials Reviews, 2017. 62(1): p. 1-31.
7. Y. Hua, R. Barker, and A. Neville, Understanding the Influence of SO_2 and O_2 on the Corrosion of Carbon Steel in Water-Saturated Supercritical CO_2. Corrosion, 2015. 71(No.5): p. 667-683.
8. Y. Hua, R. Barker, and A. Neville, The influence of SO_2 on the tolerable water content to avoid pipeline corrosion during the transportation of supercritical CO_2. International Journal of Greenhouse Gas Control, 2015. 37: p. 412-423.
9. Sun, C., Y. Wang, J. Sun, X. Lin, X. Li, H. Liu, and X. Cheng, Effect of impurity on the corrosion behavior of X65 steel in water-saturated supercritical CO_2 system. The Journal of Supercritical Fluids, 2016. 116: p. 70-82.
10. Sun, C., J. Sun, Y. Wang, X. Lin, X. Li, X. Cheng, and H. Liu, Synergistic effect of O_2, H_2S and SO_2 impurities on the corrosion behavior of X65 steel in water-saturated supercritical CO_2 system. Corrosion Science, 2016.
11. Y. Xiang, Z. Wang, C. Xu, C.C. Zhou, Z. Li, and W.D. Ni, Impact of SO_2 concentration on the corrosion rate of X70 steel and iron in water-saturated supercritical CO_2 mixed with SO_2. The Journal of Supercritical Fluids, 2011. 58(2): p. 286-294.

12. Hua, Y., R. Jonnalagadda, L. Zhang, A. Neville, and R. Barker, Assessment of general and localized corrosion behavior of X65 and 13Cr steels in water-saturated supercritical CO_2 environments with SO_2/O_2. International Journal of Greenhouse Gas Control, 2017. 64: p. 126-136.
13. Brown, J., B. Graver, E. Gulbrandsen, A. Dugstad, and B. Morland, Update of DNV recommended practice RP-J202 with focus on CO_2 corrosion with impurities. Energy Procedia, 2014. 63: p. 2432-2441.
14. Y. Hua, R. Barker, and A. Neville, The effect of O_2 content on the corrosion behaviour of X65 and 5Cr in water-containing supercritical CO_2 environments. Applied Surface Science, 2015. 356: p. 499-511.
15. N. Spycher, K. Pruess, and J. Ennis-King, CO_2-H_2O mixtures in the geological sequestration of CO_2. I. Assessment and calculation of mutual solubilities from 12 to 100℃ and up to 600 bar. Geochimica et Cosmochimica Acta, 2003. 67(16): p. 3015-3031.
16. ASTM, Standard G1-03, Standard practice for preparing, cleaning, and evaluating corrosion test specimens. ASTM International: West Conshohocken, PA, 2003.
17. ASTM, Standard G46-94, Standard guide for examination and evaluation of pitting corrosion. ASTM International: West Conshohocken, PA, 2003.